Saturation vapor pressure characterization of selected low-volatility organic compounds using a residence time chamber

Zijun Li[1,4], Noora Hyttinen[2], Miika Vainikka[1], Olli-Pekka Tikkasalo[3], Siegfried Schobesberger[1], and Taina Yli-Juuti[1]

[1]Department of Technical Physics, University of Eastern Finland, Kuopio, Finland

[2]Department of Chemistry, Nanoscience Center, University of Jyväskylä, Jyväskylä, Finland

[3]Natural Resources Institute Finland (Luke), Helsinki, Finland

[4]International Laboratory for Air Quality and Health, School of Earth and Atmospheric Sciences, Queensland University of Technology, Brisbane, Australia

Correspondence to: Zijun Li (zijun.li@qut.edu.au) and Taina Yli-Juuti (taina.yli-juuti@uef.fi)

Abstract

Saturation vapor pressure (p_{sat}) is an important thermodynamic property regulating the gas-to-particle partitioning of organic compounds in the atmosphere. Low-volatility organic compounds (LVOCs), with sufficiently low p_{sat} values, primarily stay in the particle phase and contribute to aerosol formation. Accurate information on the p_{sat} of LVOCs would require volatility measurements performed at temperatures relevant to atmospheric aerosol formation. Here, we present an isothermal evaporation method using a residence time chamber to measure p_{sat} for dry, single-compound nanoparticles at 295 K. Our method is able to characterize organic compounds with p_{sat} spanning from 10^{-8} to 10^{-4} Pa at 295 K. The compounds included four polyethylene glycols (PEG: PEG6, PEG7, PEG8 and PEG9), two monocarboxylic acids (palmitic acid and stearic acid), two dicarboxylic acids (azelaic acid and sebacic acid), two alcohols (meso-erythritol and xylitol), and one ester (di-2-ethylhexyl sebacate). There was a good agreement between our measured p_{sat} values and those reported by previous volatility studies using different measurement techniques, mostly within one order of magnitude. Additionally, quantum-chemistry-based COSMO*therm* calculations were performed to estimate the p_{sat} values of the studied compounds. COSMO*therm* predicted the p_{sat} value for most of the studied compounds within one order of magnitude difference between the experimental and computational estimates.

1. Introduction

Secondary organic aerosol (SOA) particles account for 64 % to 95 % of submicron organic aerosol particles measured at different locations from urban to remote areas (Zhang et al., 2007; Jimenez et al., 2009). Gas-phase oxidation of volatile organic compounds leads to ranges of organic vapors with different functionalities and thus, volatility. Organic vapors with sufficiently low volatility can condense onto existing particles or form new particles (Hallquist et al., 2009). Particular attention has been paid to low-volatility organic compounds (LVOCs) which significantly contribute to SOA formation (Ehn et al., 2014; Mohr et al., 2019; Schwantes et al., 2019). Under gas-

particle equilibrium, nearly all ($\approx 100\%$) LVOCs partition into the particle phase in the presence of ambient aerosol mass loadings. The volatility of an organic compound can be quantified by its saturation vapor pressure (p_{sat}) which is the key thermodynamic property describing the equilibrium gas-particle partitioning of the compound (Pankow, 1994). LVOCs typically refer to organic compounds with p_{sat} between 10^{-8} and 10^{-6} Pa (saturation mass concentration of the order between 10^{-3} and 10^{-1} µg m^{-3}). Numerous measurement techniques have been used to estimate the p_{sat} values of organic compounds (e.g., dicarboxylic acids) (Bilde et al., 2015).

The thermal desorption method is typically achieved by the desorption of particle samples from a collection plate at elevated temperature and the follow-up gas-phase measurements of the evaporating molecules with mass spectrometers. Examples of this method include the thermal desorption particle beam mass spectrometry (TDPB-MS; Chattopadhyay and Ziemann (2005)), thermal desorption proton transfer reaction mass spectrometry (TPD-PT-RMS; Cappa et al. (2008), Holzinger et al. (2010), and Eichler et al. (2015)), atmospheric solids analysis probe mass spectrometry (ASAP-MS; Bruns et al. (2012)), and Filter Inlet for Gases and AEROsols coupled with time-of-flight chemical ionization mass spectrometer (FIGAERO-ToF-CIMS; Lopez-Hilfiker et al. (2014)). Estimation of p_{sat} using the thermal desorption method can be biased by either high sample mass loading (i.e., in order of micrograms) (Huang et al., 2018) or thermal decomposition of heat-labile organic compounds (Schobesberger et al., 2018; Yang et al., 2021).

For the method based on particle size changes, a population of monodisperse particles are placed in a non-equilibrium condition so that their particle sizes decrease due to evaporation. Typically, a tandem differential mobility analyzer (TDMA) is used to monitor particle size changes during evaporation with residence times from seconds to minutes. Such a method can determine the volatilities of organic compounds with p_{sat} as low as 10^{-6} Pa (Bilde et al., 2003). The size-selected particles are in the size range from several tens to hundreds of nanometers, with number concentrations from several tens to thousands per cm^3. Flow tube-TDMA (FT-TDMA) has been deployed to probe the p_{sat} from the evaporation of dry particles or aqueous droplets under ambient temperature and relative humidity (RH) conditions (Koponen et al., 2007; Yli-Juuti et al., 2013; Emanuelsson et al., 2016). Furthermore, working at elevated temperatures up to 573 K, volatility-TDMA (V-TDMA) has been used to probe not only p_{sat} but also enthalpy of vaporization or sublimation of organic compounds by passing dry aerosol particles through a stainless steel thermodenuder at different controlled temperatures (Salo et al., 2010). To absorb the evaporated gas molecules from particle samples, the thermodenuder can be either filled up with activated charcoal (Saha et al., 2015) or followed by an activated charcoal scrubber (Salo et al., 2010). Since V-TDMA measurements are performed with elevated temperatures, the p_{sat} values derived from the measurements of thermally labile compounds can be potentially biased by thermal decomposition, as in the thermal desorption method mentioned above.

Furthermore, an electrodynamic balance (EDB) (Zardini and Krieger, 2009) or optical tweezer (Cai et al., 2015) can be used to determine the p_{sat} of organic compounds, in a manner similar to the TDMA method, by monitoring the size changes of trapped single, micrometer-sized particles. A single particle typically in the size range of 2 – 20 µm is trapped in an environmental cell. As the cell is continuously flushed with clean air flow of controlled temperature and RH, organic molecules keep evaporating from particle phase to gas phase in a non-equilibrium condition and the particle size decreases accordingly. The p_{sat} of an organic compound can be determined by the

optical measurement of particle size changes during evaporation (Zardini et al., 2006; Mitchem and Reid, 2008). For organic molecules with p_{sat} of 10^{-6} Pa or lower, using the single particle method would take more than 24 hours to obtain measurable particle size changes with minimum size measurement errors (Cai et al., 2015; Krieger et al., 2018).

Different from the TDMA method, an integrated volume method (IVM) developed by Saleh et al. (2008) estimates p_{sat} of organic compounds on the basis of the change in the total aerosol volume under a quasi-equilibrium condition. In a typical measurement, dry, polydisperse particles pass through a thermodenuder with no absorbing material and reach equilibration with the surrounding air at a set temperature, thereby leading to changes in particle size and volume. The equilibrium condition is ensured by applying high aerosol mass concentrations (~ 500 μg m^{-3}) to saturate the gas phase, and residence times of tens of seconds to complete the evaporation kinetics, with no interaction between the investigated compounds and wall material of the thermodenuder (Saleh et al., 2008). Since saturating the gas phase is essential in the IVM method, it might be challenging to apply such a method to investigate compounds of high volatilities even with mass loading of hundreds of μg m^{-3}. So far, the IVM method has been used to characterize the volatilities of atmospheric-relevant organic compounds with p_{sat} (298 K) between 10^{-5} and 10^{-4} Pa (Saleh et al., 2008; Saleh et al., 2010; Babar et al., 2020).

Knudsen cells can be also utilized for p_{sat} measurements of organic compounds. A macroscopic particle sample will be first placed in the cell with operation pressure of 10^{-2} Pa or below and then allowed to establish an equilibrium with the gas phase. The p_{sat} of an organic compound can be determined by measuring either the mass change with a mass balance over time (Da Silva et al., 2001) or effusion rate of gas-phase organic molecules from the cell with a mass spectrometer (Booth et al., 2009; Dang et al., 2019; Shelley et al., 2020). Using a mass balance as the detection method typically requires the experiments at elevated temperatures (e.g., up to 421 K) to ensure sufficient material loss from samples with p_{sat} (298 K) as low as 10^{-8} Pa (Goldfarb and Suuberg, 2008). The p_{sat} measurements using this technique can be biased if the particle samples are contaminated by compounds of high volatilities (Bilde et al., 2015). When using a mass spectrometer that has high sensitivity as the detection method, volatility measurements can be performed at around ambient temperatures (298 – 338 K) (Booth et al., 2009). So far, such a technique has been used to study organic compounds with p_{sat}(298 K) down to 10^{-6} Pa in aerosol research (Booth et al., 2009; Krieger et al., 2018).

To date, many empirical models have been developed to estimate p_{sat} of organic compounds. The simplest models use elemental compositions (Donahue et al., 2011; Bianchi et al., 2019), while group-contribution methods require knowledge on the functional groups of organic compounds (Nannoolal et al., 2008; Pankow and Asher, 2008; Compernolle et al., 2011). For a multifunctional compound, the interaction between its functional groups is an important factor for describing the intermolecular interaction in the condensed phase. The conductor-like screening model for real solvents (COSMO-RS) (Klamt, 1995; Klamt et al., 1998; Eckert and Klamt, 2002) has therefore recently been used to estimate the p_{sat} of multifunctional organic compounds that are atmospherically relevant (Kurten et al., 2016; Kurtén et al., 2018; Hyttinen et al., 2021; Hyttinen et al., 2022; Stahn et al., 2022). However, few comparisons have been made between COSMO-RS-estimated and experimental p_{sat} values of LVOCs, due to the scarcity of reliable p_{sat} measurements of relevant compounds.

Experimentally determining p_{sat} of LVOCs is challenging. All the measurement techniques presented above have their pros and cons, and multiple techniques are needed to obtain a comprehensive view on the p_{sat}. Similarly new methods for determining p_{sat} are desired, especially for measuring p_{sat} of LVOCs that are particularly relevant for atmospheric SOA formation. In this study, we present an isothermal particle evaporation method using a TDMA setup for p_{sat} characterization. Without any additional heating, the method can determine p_{sat} values of LVOCs down to 10^{-8} Pa by monitoring the evaporation of monodisperse nanoparticles in a residence time chamber (RTC) under dry conditions at room temperature (i.e., 295 K) within timescales of hours. No calibrant with known p_{sat} is required. The RTC method has been also used to study volatilities of biogenic SOA particles in previous studies (Yli-Juuti et al., 2017; Buchholz et al., 2019; Li et al., 2019; Li et al., 2021; Li et al., 2023). Different from our RTC approach, Cain et al. (2020) used a dilution chamber filled with clean air to isothermally dilute the polydisperse aerosol particles by a factor of 10 to initiate particle evaporation. Using the approach of Cain et al. (2020) to estimate particle volatility requires corrections for size-dependent particle wall-loss and coagulation.

Here we used the RTC method to study a set of LVOCs of which p_{sat} values have been reported in literature. Moreover, quantum chemistry calculations with COSMO-RS were performed to estimate p_{sat} values of the selected LVOCs. A comparison between experimental and calculated p_{sat} values helps us evaluate the accuracy of the p_{sat} calculations of the studied LVOCs.

2. Methods

2.1. Particle evaporation measurements

In this study, a set of pure organic compounds were chosen for p_{sat} characterization and used as received without any purification. The used polyethylene glycol (PEG, Polypure AS) standards were PEG6, PEG7, PEG8, and PEG9. The used mono- and dicarboxylic acids were palmitic acid (Sigma Aldrich, ≥ 99%), stearic acid (Sigma Aldrich, 95%), azelaic acid (Sigma Aldrich, 98%), and sebacic acid (Sigma Aldrich, 99%). The remaining chemicals were meso-erythritol (Alfa Aesar, 99%), xylitol (Sigma Aldrich, ≥ 99%) and di-2-ethylhexyl sebacate (DEHS, Topas GmbH, > 98%). The properties of individual organic compounds are summarized in Table 1. Acetonitrile (Fisher Scientific, 99.8%) was used as a solvent for stock solutions in this study, with the exception of meso-erythritol and xylitol which were dissolved using deionized water (18.2 MΩ).

Table 1. Properties of the organic compounds used in this study.

Groups	Compounds	Chemical Formula	M [a] [g mol^{-1}]	ρ [b] [g cm^{-3}]	σ [c] [mN m^{-1}]	D_{air} [d] [m^2 s^{-1}]
Polyethylene Glycol	PEG 6	$C_{12}H_{26}O_7$	282.30	1180	45	4.67×10^{-6}
	PEG 7	$C_{14}H_{30}O_8$	326.40	1206	45	4.32×10^{-6}
	PEG 8	$C_{16}H_{34}O_9$	370.40	1234	45	4.04×10^{-6}
	PEG 9	$C_{18}H_{38}O_{10}$	414.50	1257	45	3.80×10^{-6}
Monocarboxylic acid	Palmitic acid	$C_{16}H_{32}O_2$	256.42	852	130	4.37×10^{-6}
	Stearic acid	$C_{18}H_{36}O_2$	284.48	941	160	4.12×10^{-6}

Dicarboxylic acid	Azelaic acid	$C_9H_{16}O_4$	188.22	1251	180	5.65×10^{-6}
	Sebacic acid	$C_{10}H_{18}O_4$	202.25	1210	100	5.38×10^{-6}
Alcohol	meso-Erythritol	$C_4H_{10}O_4$	122.12	1451	160	7.66×10^{-6}
	Xylitol	$C_5H_{12}O_5$	152.15	1520	160	6.85×10^{-6}
Ester	DEHS	$C_{26}H_{50}O_4$	342.30	912	32	3.37×10^{-6}

[a] molecular weight; [b] density, for references see Table S1 in the Supplement; [c] surface tension or energy, for references see Table S2 in the Supplement; [d] gas-phase diffusivity of a compound in air calculated using Eq. (2).

Particle samples were generated by nebulizing solutions of organic compounds with an atomizer (ATM 226, Topas GmbH). Prior to the size selection, either a silica gel diffusion dryer or a large dilution flow of dry purified air was used to remove the used solvent (i.e., water or acetonitrile). The schematic diagram of the measurement setup is shown in Figure S1 in the Supplement. Two parallel nanometer aerosol mobility analyzers (NanoDMA, model 3085, TSI) were used to select particles with 80-nm electrical mobility diameter. We operated the two NanoDMAs in an open-loop setting with a sample to sheath flow ratio of 1:8 with clean, dry air as the sheath flow. Such a configuration ensured the gas phase free of the studied compounds (Li and Chen, 2005). Eventually, the resultant monodisperse aerosol was fed into either bypass lines of varying lengths or into a stainless-steel RTC of either 25 L or 100 L in volume for prolonged isothermal evaporation. This setup for particle evaporation measurements enables residence times from one second to nearly seven hours. Vapor wall losses in the bypass lines and RTCs were rapid enough to ensure negligible amounts of vapors in the gas phase (Yli-Juuti et al., 2017). The whole setup was maintained under dry conditions (RH < 5%) at 295 K. Before each isothermal evaporation experiment, the NanoDMAs, bypass tubing, and RTCs were flushed for hours with dry purified air.

Particle size changes due to isothermal evaporation were periodically measured with a scanning mobility particle sizer (SMPS, TSI; DMA 3080, CPC 3775). Under the assumption of particle sphericity, the extent of particle evaporation was quantified using the evaporation factor (EF). Independent of particle number concentration or mass loading, the EF was determined as $(D_{p,t}/D_{p,0})$. We chose the measured size with the least amount evaporation (residence time = 1s following size selection) as $D_{p,0}$ and the measured size after residence time t of evaporation as $D_{p,t}$.

2.2. Determination of p_{sat} values

For each of the studied compound, the p_{sat} value can be determined from the isothermal evaporation data (Riipinen et al., 2006; Salo et al., 2010). The particle size change due to evaporation can be expressed as

$$\frac{dD_p}{dt} = -p_{sat} \cdot \frac{4D_{i,air}M_i}{\rho_i D_p RT} \cdot \exp\left(\frac{4\sigma_i M_i}{\rho_i D_p RT}\right) \cdot \beta, \qquad (1)$$

where $D_{i,air}$ is the gas-phase diffusivity of molecule i in air, M_i is the molecular weight, ρ_i is the density, R is the universal gas constant, T is the temperature (i.e., 295 K), σ_i is the surface tension or energy, and β is a factor correcting the condensation mass flux in the transition regime (D_p in between 0.02 and 3 µm).

The gas-phase diffusivity of molecule i in air, $D_{i,air}$, can be estimated using Fuller's semi-empirical method (Fuller et al., 1966)

$$D_{i,air} = \frac{10^{-3}T^{1.75}(\frac{1}{M_i}+\frac{1}{M_{air}})^{0.5}}{P(\sqrt[3]{V_i}+\sqrt[3]{V_{air}})^2}, \tag{2}$$

where p is the experimental pressure (i.e., 1 atm) and M_{air} is the molecular weight of air. In addition, V_i and V_{air} are the corresponding diffusion volumes for molecules i and air. For a molecule, the diffusion volume can be calculated by adding the diffusion volumes of all the atoms. Here we used 15.9 for C, 2.31 for H, and 6.11 for O (Reid et al., 1987).

For the transition regime correction factor β, we used Fuchs-Sutugin approximation to describe the gas diffusion in the transition regime (Fuchs and Sutugin, 1971):

$$\beta = \frac{1+Kn}{1+0.3773 \cdot Kn + 1.33 \cdot Kn \cdot (\frac{1+Kn}{\alpha})}, \tag{3}$$

where Kn is the Knudsen number and α is the accommodation coefficient. Chamber partitioning studies (Krechmer et al., 2017; Liu et al., 2019) and molecular dynamics simulations (Julin et al., 2014; Von Domaros et al., 2020) suggested that α was close to unity for LVOCs, and thus α was set to unity in this study. Kn is two times the ratio between the mean free path of the molecule i in air ($\lambda_{i,air}$) and particle diameter (D_p):

$$Kn = \frac{2\lambda_{i,air}}{D_p}, \tag{4}$$

The value of $\lambda_{i,air}$ can be further expressed following Fuchs and Sutugin (1971):

$$\lambda_{i,air} = \frac{3D_{i,air}}{\overline{c_i}}, \tag{5}$$

where $\overline{c_i}$ is the mean speed of a molecule of i in pure gas of i. For a molecule i, the value of $\overline{c_i}$ can be described as follows (Moore, 1962)

$$\overline{c_i} = \sqrt{(\frac{8RT}{\pi M_i})}, \tag{6}$$

The p_{sat} value for each organic compound was estimated using Approximate Bayesian Computation with Sequential Monte Carlo (ABC-SMC) (Sisson et al., 2007; Toni et al., 2009; Liepe et al., 2014). The ABC-SMC algorithm for a single parameter (i.e., p_{sat}) works by first drawing samples of p_{sat} from a pre-determined prior distribution. For each sample of p_{sat}, a loss function is used to measure the difference between the simulation based on Eq. (1) and observed evaporation data. Only those samples which have their computed losses below the acceptance threshold (ε_1) will be accepted, resulting in the first posterior distribution of sample size N. Subsequently, new samples are drawn from the previous posterior distribution with a probability proportional to a weight and then are perturbed as in Toni et al. (2009). Applying the defined loss function and a smaller acceptance threshold ($\varepsilon_2 < \varepsilon_1$), we produce a new posterior distribution of N samples of p_{sat}. The procedure of generating a new set of N accepted samples from the previous posterior distribution is repeated for J times with always decreasing acceptance thresholds ($\varepsilon_J < \varepsilon_{J-1}$

$< .... < \varepsilon_2 < \varepsilon_1$). This finally leads to an estimate which can be approximated as the true p_{sat} of the compound of interest given the observed particle evaporation data.

195   The ABC-SMC sampling process was performed using the Python package pyABC (Klinger et al., 2018). For each organic compound, the mean value of p_{sat} and the 95% credible interval (CrI) were calculated using all accepted samples from the final set of N samples at the end of the pyABC run. The sample size N was defined as 500. The number of iterations typically ranges from 10 to 30 (Schälte and Hasenauer, 2020), and here we set the iteration time J to 10. The prior distribution was set to be a log-uniform distribution between 10^{-10} and 10^{-3} Pa.

200   Sum of the squared residuals between the observed and simulated evaporation data was defined as the loss function. The number of data points with residence time longer than one hour was typically less than the number of data points with residence time of one hour or less. To prevent data points with short residence times from dominating the fittings, the squared difference for each data point with residence time longer than one hour was scaled with a scaling factor that was the number of data points with residence times of one hour or less. The minimum acceptance

205   threshold was defined as the total sum of the maximum uncertainties ($\pm 1.875\%$ in particle size) from all observation data points. By default, the acceptance thresholds (ε_1 to ε_J) are automatically calibrated and updated in pyABC. The sampling in pyABC was terminated once either the minimum acceptance threshold or maximum number of iterations (i.e., here set to 10) was reached, whichever came first.

2.3.   Quantum chemical calculations using COSMO*therm*

210   Conductor-like screening model for real solvents (COSMO-RS; Klamt (1995); Klamt et al. (1998); Eckert and Klamt (2002)) uses a combination of quantum chemistry and statistical thermodynamics to estimate condensed-phase thermodynamic properties, e.g., p_{sat} of pure compounds. The COSMO-RS model is implemented in the COSMO*therm*2021 program (BIOVIA COSMO*therm*, 2021), where the model has been parameterized using experiments of a large set of compounds. The COSMO*therm*2021 program was used to calculate the p_{sat} of the

215   organic compounds. The input files for mono- and dicarboxylic acids and alcohols were taken from the COSMO*base*2021, which contains COSMO*therm* input files of most commonly used compounds. Input files for the other compounds (i.e., DEHS, PEGs) were generated using the BP-TZVPD-FINE-COSMO+GAS_18 template of COSMO*conf*2021 (BIOVIA COSMO*conf*, 2021), which has been created for finding suitable conformer sets for COSMO*therm* calculations. The density functional theory calculations were performed using the TURBOMOLE

220   program version 7.4.1 (Turbomole, 2019). In COSMO*therm*, we used the BP_TZVPD_FINE_21 parametrization and 295 K temperature. For each compound, the p_{sat} in the subcooled liquid state (p_{sat}^l) is calculated using its free energy values in the gas (G^g) and pure liquid phases (G^l):

$$p_{sat}{}^l = e^{-\frac{\left(G^l - G^g\right)}{RT}} \tag{7}$$

Some of the studied compounds can be crystalline solid in bulk at the experimental temperature (i.e., 295 K), which

225   needs to be considered in the p_{sat} calculations. COSMO*therm* is able to estimate saturation vapor pressures in the crystalline solid state (p_{sat}^s), if experimental melting temperatures and heats of fusion are given as input. The experimental melting temperatures and heats of fusion used in the COSMO*therm* calculations are correspondingly listed in Tables S3 and S4 in the Supplement. The free energy of fusion (ΔG_{fus}) at the given temperature is calculated

from the given experimental values of melting temperature and enthalpy of fusion and added to the free energy of

230 vaporization. For each compound, its p_{sat}^s can be estimated as follows:

$$p_{sat}^s = e^{-\frac{\left(G^l - G^g - \Delta G_{fus}\right)}{RT}}$$ (8)

3. Results and discussion

With the use of the ABC-SMC method to optimize the evaporation model, we determined the p_{sat} values from the data points collected in the isothermal evaporation measurements under dry conditions at 295 K. The optimized p_{sat}

235 values for the studied compounds are summarized in Table 2. In the following sections for each compound group, we also included the p_{sat} values (at 298 K) reported by previous studies for systematic comparisons. Details of each included study can be found in the Tables S6-S12 in the Supplement. Similar to Bilde et al. (2015), we used two different symbols to distinguish p_{sat} measurements assumed to be taken in crystalline solid or liquid states. In Figures 1e, 2 and 4, filled squares indicate p_{sat} values assumed to be measured in a crystalline solid state, while

240 open circles represent p_{sat} values assumed to be measured in a liquid state.

Note that there could be uncertainties from the chosen sets of α and σ for individual compounds. To examine their impacts on the estimated p_{sat} values, we performed several sensitivity analyses as shown in Figures S2 – S6 of the Supplement. As α decreased, the estimated p_{sat} values increased by a factor of two for $\alpha = 0.5$ and increased by a factor of nine for $\alpha = 0.1$, compared with those estimated with $\alpha = 1$. When varying σ by $\pm 50\%$, we found mostly

245 small, and in all cases below one order of magnitude, changes in the estimated p_{sat} values for all three tested values of α. Previous experimental (Krechmer et al., 2017; Liu et al., 2019) and computational works (Julin et al., 2014; Von Domaros et al., 2020) have suggested that α is close to unity for the LVOC category, which the selected compounds of this study fall into. Therefore, the optimized p_{sat} values were estimated using $\alpha = 1$ and the presented uncertainty ranges for p_{sat} include $\pm 50\%$ variation in the chosen σ and the fitting uncertainties (i.e., 95 % CrIs).

250 Dependent on the studied compounds, the contributions of the fitting uncertainties to the presented uncertainty ranges varied from 3% to 95%.

Table 2. Summary of p_{sat} at 295 K for the organic compounds measured in this study.

Groups	Compounds	p_{sat} [Pa][a]
Polyethylene Glycol	PEG 6	$2.24^{+0.50}_{-0.39} \times 10^{-5}$
	PEG 7	$1.06^{+0.21}_{-0.17} \times 10^{-6}$
	PEG 8	$6.51^{+1.25}_{-1.06} \times 10^{-8}$
	PEG 9	$6.71^{+9.75}_{-3.86} \times 10^{-9}$
Monocarboxylic acid	Palmitic acid	$5.40^{+3.94}_{-2.30} \times 10^{-6}$
	Stearic acid	$2.42^{+1.97}_{-1.09} \times 10^{-7}$
Dicarboxylic acid	Azelaic acid	$7.61^{+5.16}_{-3.13} \times 10^{-6}$
	Sebacic acid	$1.07^{+0.23}_{-0.19} \times 10^{-7}$
Alcohol	meso-Erythritol	$3.75^{+1.15}_{-0.81} \times 10^{-5}$
	Xylitol	$1.71^{+0.48}_{-0.37} \times 10^{-6}$
Ester	DEHS	$7.52^{+1.81}_{-1.46} \times 10^{-7}$

[a] The optimized p_{sat} values were estimated using $\alpha = 1$, and the presented uncertainty ranges for p_{sat} include $\pm 50\%$ variation in the chosen σ and the fitting uncertainties (i.e., 95 % CrIs).

3.1. Polyethylene glycols (PEGs)

The measured and simulated EFs of the four PEG compounds are shown in Figure 1a – d. For the remaining compounds, the measured and simulated EFs can be found in Figures S7 – S10 in the Supplement. With increasing monomer units, the PEG particles showed slower evaporation rates and thus lower volatilities, as expected based on previous measurements (Krieger et al., 2018) and in agreement with their increasing maximum desorption temperatures measured by FIGAERO-CIMS (Ylisirniö et al., 2021). For the investigated PEGs, the p_{sat} values at 295 K were estimated to be in the range between 10^{-9} and 10^{-4} Pa. Bulk PEG6 – 8 were in liquid states at the experimental temperature which was above or close to their melting points (Table S3). Given the waxy form of PEG9 at the experimental temperature of 295K, PEG9 particles were most likely in an amorphous solid state and, therefore, the p_{sat} value of PEG9 from our study should be close to that of the subcooled liquid (Bilde et al., 2015). Among these four PEGs, the estimated p_{sat} value of PEG9 has the largest relative uncertainty. This is due to the relatively small size changes of PEG9 particles within the experimental time scale of nearly seven hours. Compared with literature values for PEG6-9 reported by Krieger et al. (2018), our newly derived values agree within a factor of 2 (Figure 1e).
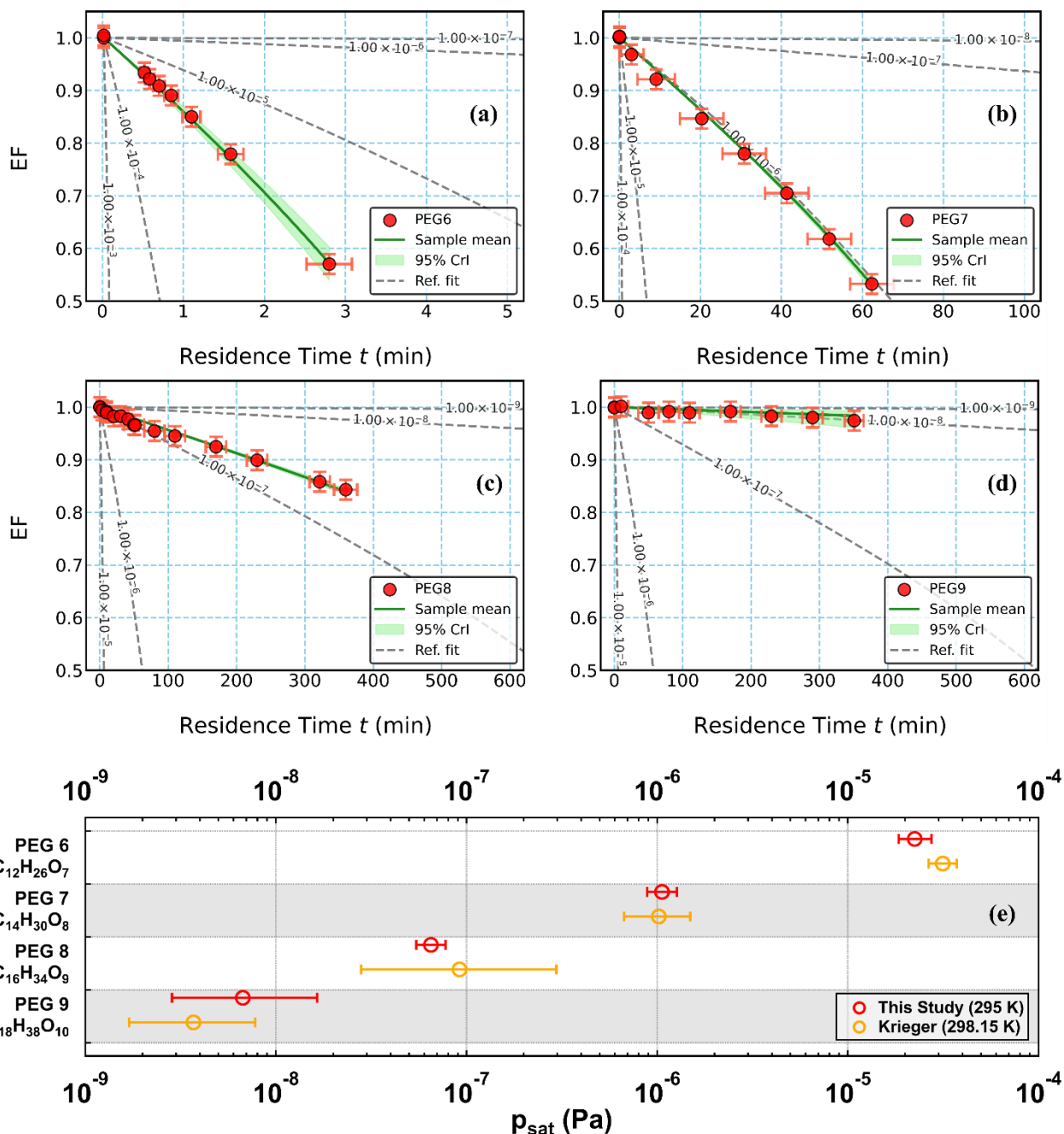
Figure 1. Panels (a) − (d): Measured evaporation factors (EFs; circles) as a function of residence time for PEGs (PEG 6 – 9), simulations with the average optimized p_{sat} values (solid green lines) and 95% credible intervals (95% CrIs; shaded areas in green), and simulated evaporation curves with a set of reference p_{sat} values (10^{-9} to 10^{-3} Pa, with one-decade intervals, dashed grey lines). All the simulated evaporation curves were computed using $\alpha = 1$ and the chosen σ shown in Table 1. For the measured data points of EF in (a) – (d), the error bars represent the maximum uncertainty of ±1.875% in particle size measurements on y-axis and the minimum and maximum residence times on x-axis. Panel (e): Measured p_{sat} values for PEGs in this study (red) together with the those reported by Krieger et al. (2018) (yellow). For the p_{sat} values from this study, they were estimated using $\alpha = 1$, with error bars including ± 50% variation in the chosen σ and the fitting uncertainties (i.e., 95 % CrIs).

3.2. Mono- and dicarboxylic acids

For the mono- and dicarboxylic acids, the measured p_{sat} values from this study and previous studies are depicted in Figure 2a – d. Our results are in the range between 10^{-7} and 10^{-5} Pa at 295 K. All these four compounds have melting points higher than the experimental temperature (Table S3) and therefore the p_{sat} values are here assumed to correspond to solid, crystalline phase, although subcooled liquid phase cannot be ruled out. For each of the four carboxylic acids, the p_{sat} value from this study is in the range of values reported by other independent measurements (Figure 2a – d, b). Among all studies compared in Figure 2, Cappa et al. (2007) and Cappa et al. (2008) reported the lowest solid p_{sat} values from their measurements (Figure 2a – d; bottom rows). Different from other studies, they particularly preheated the particle samples for 30 – 60 min at a temperature slightly above the melting points, in order to remove any solvent molecules which could remain in the particles after sample preparation. Prior to the p_{sat} characterization with the temperature-programmed desorption, the preheated samples were cooled down to 273 K to ensure the particle samples to be in crystalline solid states.

It has been suggested that quick drying after atomization of aqueous organic droplets might not be sufficient to remove all solvents out from the particles (Bilde et al., 2015). Cappa et al. (2007) concluded that the retained solvent molecules might: 1) disrupt the crystal structure at the sample surface to allow many carboxylic acid molecules to exist in configurations favoring evaporation; and 2) increase surface areas for evaporation by increasing surface roughness and porosity. These two effects would possibly increase the evaporation rates of the studied carboxylic acid molecules. For instance, the crystalline-solid p_{sat} values of palmitic acid from our study and other three independent measurements (Davies and Malpass (1961); Tao and Mcmurry (1989); Chattopadhyay and Ziemann (2005)), which used atomized samples after quick drying, are much higher than the crystalline-solid p_{sat} values from samples with less likely impact from solvent molecules (Cappa et al., 2008; Yatavelli and Thornton, 2010) but very close to the liquid p_{sat} value which was predicted by Cappa et al. (2008) based on their crystalline-solid p_{sat} value (Figure 2a). Different from palmitic acid, our crystalline-solid p_{sat} value of stearic acid from atomized samples is very close to the crystalline-solid p_{sat} value but not the liquid one reported by Cappa et al. (2008) (Figure 2b). Furthermore, Saleh et al. (2010) found very similar p_{sat} values of azelaic acid between two sample types which were prepared using atomization (thereby involving solvent; labelled with (a)) and homogeneous condensation (involving no solvent; labelled with (b)) (Figure 2c).

To assess whether retention of solvents impacted our measured p_{sat} values, we normalized the crystalline-solid p_{sat} values from other studies (excl. Bilde et al. (2015)) to the one obtained in our study for comparison, as shown in Figure 3. Depending on the studied carboxylic acid, the range of the reported p_{sat} values (grey bars) spans from over one order of magnitude to almost four orders of magnitude. We further categorized studies into two groups according to how the particle samples were prepared. Descriptions of sample preparation in different studies can be found in Tables S7-S10 in the Supplement. In the first group we included studies where aerosol particles were generated by atomization followed by quick drying, while in the second group we included studies where additional procedures (e.g., preheating, homogenous nucleation) were applied to eliminate the solvents from the samples. In general, the group potentially impacted by solvent (blue bar) has higher normalized p_{sat} values, compared the group with no impact from solvent (yellow bar). Divisions between the two sample groups are clearly observed in the two dicarboxylic acids but not in the two monocarboxylic acids. Whether the impact of retained solvent molecules

on p_{sat} measurements is compound-dependent or not would require further investigations with more organic compounds.

Among the studied carboxylic acids, the span of the measured p_{sat} values for azelaic acid is relatively large, even when only considering those studies with no impact from solvent molecules. As azelaic acid is a dicarboxylic acid with nine carbon atoms, polymorphism is one potential factor to be considered when comparing the p_{sat} values between different studies. Previous thermal desorption measurements suggested the presence of polymorphism in dicarboxylic acids with odd number of carbon atoms ($\leq$ 9) (Chattopadhyay and Ziemann, 2005; Salo et al., 2010) as bimodal size distribution was observed during particle evaporation at elevated temperatures (313 – 333 K). However, we did not observe any bimodal distributions of evaporating particles for azelaic acid in the present study that was carried out at 295 K.
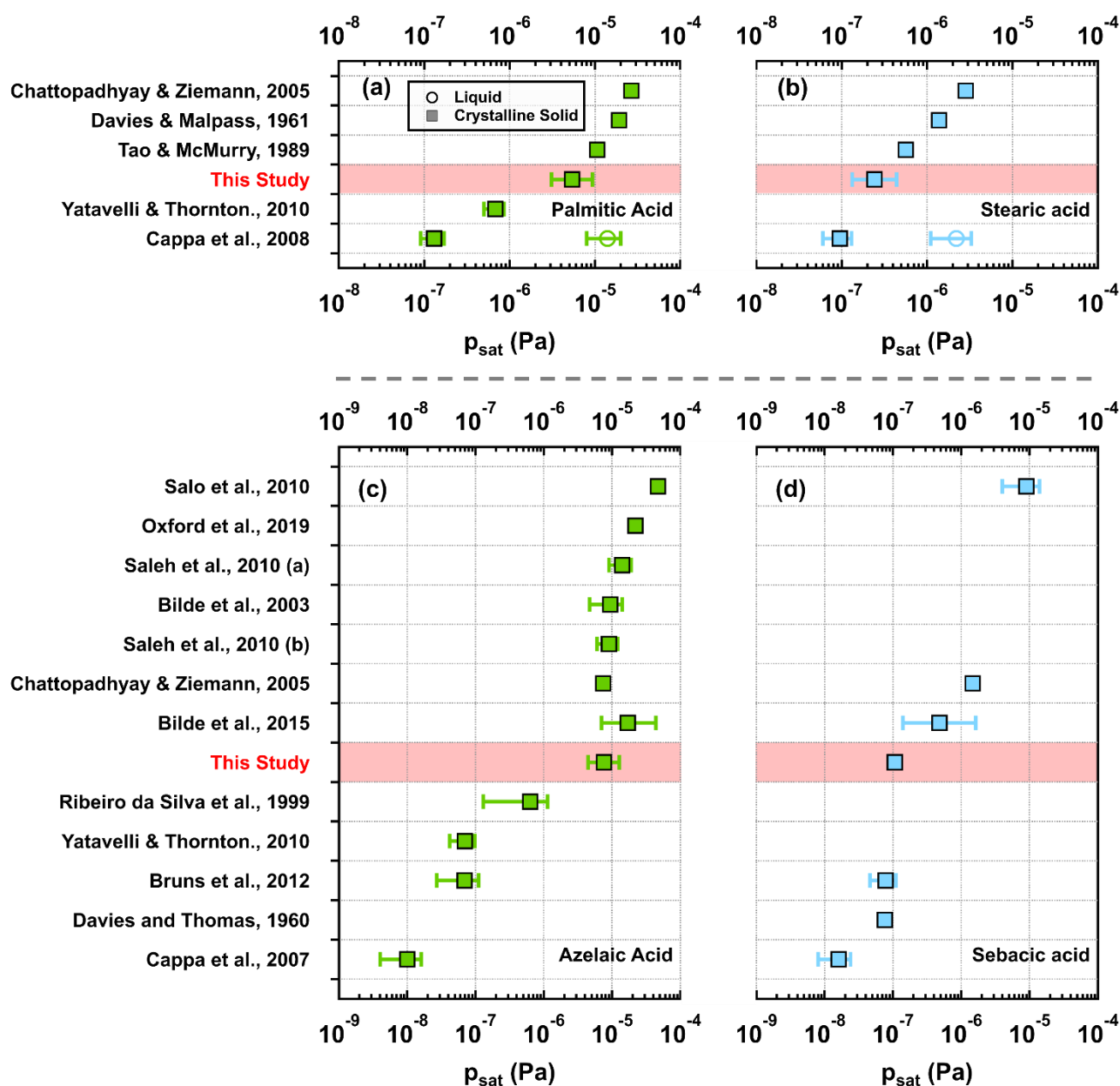
Figure 2. Measured p_{sat} values from this study (rectangle in red shaded area) together with those reported in literature for palmitic acid (a; green), stearic acid (b; blue), azelaic acid (c; green), and sebacic acid (d; blue). Note that the p_{sat} values and their uncertainties from Bilde et al. (2015) were based on the combined data sets of different studies but not from a particular study or experimental method. For the p_{sat} values from this study, they were estimated using $\alpha = 1$, with error bars including $\pm 50\%$ variation in the chosen σ and the fitting uncertainties (i.e., 95 % CrIs).
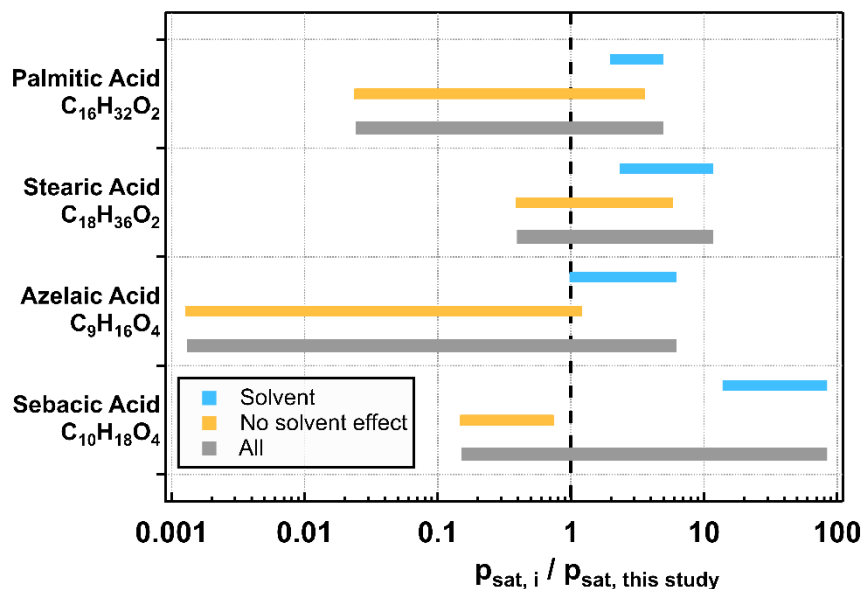
Figure 3. Ranges of normalized p_{sat} values for palmitic, stearic, azelaic, and sebacic acids. Each reported p_{sat} value in literature was normalized to that of our study. The whole range of normalized p_{sat} of each compound is shown as a grey bar. The group of samples potentially impacted by solvents is shown as a blue bar, while that with no impact from solvents is shown as a yellow bar. Note that data from Bilde et al. (2015) shown in Fig. 2 were not included for these analyses.

3.3. DEHS and Alcohols

The measured and simulated EFs for DEHS as a function of residence time are presented in Figure S4 in the Supplement. DEHS is in a liquid state at the experimental temperature which is much higher than its melting point (Table S3). The p_{sat} value from our study is $7.52^{+1.81}_{-1.46} \times 10^{-7}$ Pa for DEHS. We could not find any literature p_{sat} value for DEHS. However, dioctyl sebacate (DOS; an isomer with very similar structure) has a comparable p_{sat} value of 2.74×10^{-6} Pa at 298 K (Rader et al., 1987).

For xylitol, with an additional -CHOH- in the carbon backbone, the measured p_{sat} value is approximately one order of magnitude lower than that of meso-erythritol (Figure 4; bottom row). The p_{sat} value of meso-erythritol agrees with literature data within less than a factor of 2, while the p_{sat} value of xylitol agrees with that extrapolated from the measurement in Barone et al. (1990) within a factor of 2 (Figure 4).

The melting points of both bulk xylitol and meso-erythritol are above the experimental temperature (Table S3). However, Emanuelsson et al. (2016) observed a bimodal distribution of meso-erythritol particles after evaporation, indicative of two types of particles with different volatilities, and suggested the coexistence of crystalline solid and

liquid phases. The presence of such bimodal behavior became increasingly important with the decreasing particle size and/or increasing experimental temperature (298K: < 64 nm; 303 K: < 83 nm; 308 K: < 180 nm) (Emanuelsson et al., 2016). Cheng et al. (2015) found that aerosol particles smaller than certain critical sizes tend to remain in a liquid state, even at a temperature below the bulk phase transition temperature. However, we did not observe any

360 bimodal distributions of evaporating particles for meso-erythritol in our study. This is likely due to the fact that the particle sizes in our study were mostly larger (61 – 77 nm) than the size range (i.e., < 64 nm at 298 K) which exhibited bimodal evaporation behavior in Emanuelsson et al. (2016). Even though the bimodal behavior of evaporated meso-erythritol particles was not observed in our study, we cannot rule out the co-existence of crystalline solid and liquid phase states for the meso-erythritol particles.
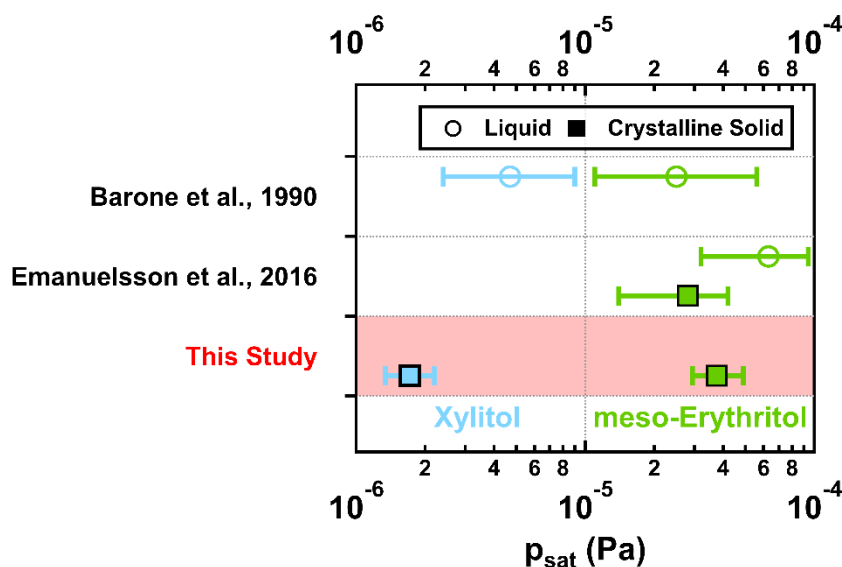
365

Figure 4. Measured p_{sat} values from this study (rectangle in red shaded area) together with those reported in literature for meso-erythritol (green) and xylitol (blue). For the p_{sat} values from this study, they were estimated using $\alpha = 1$, with error bars including $\pm 50\%$ variation in the chosen σ and the fitting uncertainties (i.e., 95 % CrIs).

3.4. Comparison with p_{sat} values derived from COSMO*therm* computations

370 The p_{sat} values of the organic compounds were estimated using COSMO*therm* calculations. The results for DEHS and PEGs were estimated with the input files generated using the COSMO*conf*2021 program, while those for the studied carboxylic acids and alcohols were computed using the input files from COSMO*base*2021. At the experimental temperature of 295 K, DEHS and the four PEGs (PEG6 – 9) remain in liquid or amorphous states for their bulk. Thus, only their corresponding p_{sat}^l values were derived from COSMO*therm*. For the remaining

375 compounds of interest (i.e., carboxylic acids, alcohols), the bulk materials are in a crystalline solid state at 295 K. We computed their p_{sat}^l values but also further derived their p_{sat}^s values by accounting for ΔG_{fus} (see Eq. (8)) for comparing with the measured p_{sat} values. For the p_{sat}^s values, we found the upper and lower limits of estimates using the lowest and highest experimental ΔG_{fus} values from literature (Table S4), respectively.

We compared the measured p_{sat} values with the p_{sat}^l and/or p_{sat}^s which were estimated by COSMO*therm*, as shown

380 in Figure 5. The p_{sat} values predicted by COSMO*therm* were in reasonable agreement with the experimental values for most of the studied compounds, when considering a reasonable difference of one log unit between

measurements and COSMO*therm* estimates. Based on bulk thermodynamics, the carboxylic acids and alcohols would be in a crystalline solid phase at the experimental temperature of 295 K. Their p_{sat}^s values better agree with the experimental values, compared with the p_{sat}^l values. Exceptions are found in the two dicarboxylic acids for which the p_{sat}^l values (blue open circles) are equally close to or agree better with the experimental p_{sat} value, compared with the p_{sat}^s values (blue filled bars). However, the COSMO*therm* systematically underpredicted the experimental p_{sat} values of PEGs by orders of magnitude. This is the opposite to a previous computational study on multifunctional compounds, where an older parametrization (BP_TZVPD_FINE_18) of COSMO*therm* was seen to overestimate the p_{sat} by a factor of 5 for every intramolecular hydrogen bond in the compound (Kurtén et al., 2018). Here, the large underestimation of the p_{sat} of the PEGs by COSMO*therm* suggests that COSMO*therm* overestimates the stability of the condensed phase relative to the gas-phase molecules.

Kurtén et al. (2018) recommended selecting conformers to COSMO*therm* calculations based on their intramolecular hydrogen bonding in order to improve the p_{sat} estimations of multifunctional compounds. The best agreement between experimental and computed p_{sat} values was found by using only conformers that contain no intramolecular hydrogen bonds in the COSMO*therm* calculations (Kurtén et al., 2018). Here we found that the conformers of multifunctional carboxylic acids and alcohols included in the COSMO*base* produce accurate p_{sat} estimates, even if conformers containing intramolecular hydrogen bonds were not excluded from the calculations. Note that the COSMO*base* conformers of the studied multifunctional carboxylic acids and alcohols were likely used in the parametrization of the p_{sat} estimates for the quantum chemistry input in the COSMO-RS model. This may explain why the conformers of COSMO*base* produce accurate p_{sat} estimates for these compounds. Systematic conformer sampling and selecting conformer based on their intramolecular hydrogen bonding, suggested by Kurtén et al. (2018), led to higher p_{sat} values (lower p_{sat} for xylitol) than the conformers of COSMO*base*, worsening the agreement with experiments (Table S13). The discrepancy between COSMO*therm*-derived and experimental p_{sat} of the PEGs may be caused by the lack of organic compounds similar to large PEGs in the set of compounds used in the BP_TZVPD_FINE_21 parametrization of COSMO*therm*.
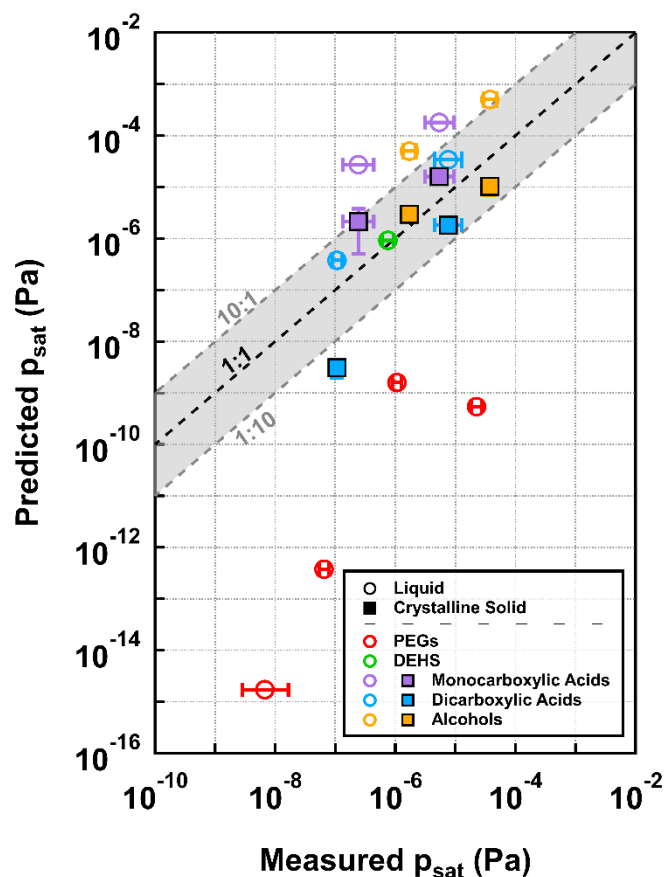
Figure 5. Comparison of p_{sat} values between the measurement in this study (x-axis) and different COSMO*therm* predictions (y-axis) at 295 K. The two different markers represent the comparisons of measured p_{sat} values with the COSMO*therm*-estimated p_{sat} values of liquid (open circles) and crystalline solid (filled squares) phase states, respectively. The error bar of each marker on x-axis represents the uncertainty range for the p_{sat} value estimated using $\alpha = 1$, which includes $\pm 50\%$ variation in the chosen σ and the fitting uncertainties (i.e., 95 % CrIs). The error bar of each filled square on y-axis shows the range between the maximum and minimum COSMO*therm*-estimated crystalline solid p_{sat} values. The dashed black line is the 1:1 line, with grey shaded areas showing a deviation of one log unit.

4. Conclusions

Here we presented a TDMA-based method to investigate the isothermal evaporation of dry organic nanoparticles that consist of a single compound in a RTC. Using this method, we characterized organic compounds with p_{sat} spanning from 10^{-8} to 10^{-4} Pa at 295 K. The experimentally determined p_{sat} values from this study are within the ranges of those reported in previous studies based on different measurement techniques. The advantage of our method is that the evaporation measurements are performed at an atmospherically relevant temperature and the ability to determine p_{sat} values down to 10^{-8} Pa in the LVOC range. We acknowledge that there could be uncertainties regarding to the particle phase state and the presence of polymorphism, which have been also discussed in previous volatility studies (Bilde et al., 2003; Chattopadhyay and Ziemann, 2005; Cappa et al., 2007; Emanuelsson et al., 2016). To address such uncertainties would require in-situ spectroscopic methods (e.g., Mie resonance spectroscopy, Raman spectroscopy) that are sensitive enough to differentiate between crystalline solid, amorphous, and subcooled liquid states (Price et al., 2022) and to identify different polymorphic forms (Yeung et

al., 2010). In addition, it has been suggested that aerosol materials with high bulk melting points would be in liquid states at room temperature, once reaching a critical diameter between 12 – 40 nm (Cheng et al., 2015). However, the experimental data on such phase changes are limited to a very small set of compounds (e.g., sodium chloride, ammonium sulfate, polystyrene). Future investigations on the size dependence of phase transitions of LVOCs should be warranted. Such knowledge will advance our understanding about the phase states but also the volatilities of LVOCs, when they exist in a particle size range (50 – 100 nm) highly relevant to cloud condensation nuclei activation (Kerminen et al., 2012). Furthermore, we found that COSMO*therm* is able to reproduce our measured p_{sat} values for the studied compounds except PEGs, mostly within one order of magnitude. The large difference between the measured and calculated p_{sat} values of PEG highlights the importance of conformer selection in COSMO*therm* calculations for new types of compounds that have not been used in the parametrization of the model. Unsuitable conformer selection may therefore lead to substantial uncertainties, especially for LVOCs that have not been used in the parameterization of the model.

The current study was focused on p_{sat} characterization for dry, single-compound particles at one set temperature. Nonetheless, our method can be further used to perform isothermal evaporation experiments at different temperature and RH settings. This will help probe two other important thermodynamics properties - enthalpy of vaporization and organic activity coefficient, which are important to the gas-to-particle partitioning of organic compounds. Furthermore, the method can be extended to study interactions between compounds in multicomponent aerosol particles, e.g., to study the matrix effect of inorganic salts and non-volatile organics on the isothermal evaporation of LVOCs (Liu et al., 2020). For atmospheric SOA particles which consist of hundreds or even thousands of compounds, their evaporation rates are regulated by the complex interplay between volatility distribution, particle viscosity and particle-phase chemistry. Previous studies with a similar experimental setup have shown biogenic SOA particle evaporation to be dependent on RH (Yli-Juuti et al., 2017), temperature (Li et al., 2019), oxidation levels (Buchholz et al., 2019), or molecular composition (Li et al., 2021; Li et al., 2023). This study, together with the previous studies on SOA particles, have shown the applicability of combining RTC experiments with process modelling. While the RTC method was here used by only probing the size changes during particle evaporation, obtaining molecular-level insights into SOA particle evaporation processes additionally require detailed composition analysis.

Data availability. The data set is available upon request from the corresponding author.

Supplement. The supplement related to this article is available online.

Author contribution. ZL designed the study. ZL and MV carried out the laboratory experiments. NH performed the COSMO*therm* calculations. ZL and OPT ran the optimization model. ZL, NH, SS, and TYJ analyzed and interpreted data. ZL wrote the paper with contributions from all coauthors.

Competing interest. The authors declare that they have no conflict of interest.

Acknowledgements: The authors would like to thank Dr. Angela Buchholz for useful assistance on the measurement setups.

Financial support. This research has been supported by the Academy of Finland Flagship program (grant no. 337550), Academy of Finland (grant nos. 317373, 338171, 346371), and the University of Eastern Finland Doctoral Program in Environmental Physics, Health and Biology. We also thank CSC - IT Center for Science, Finland, for computational resources.

References

Babar, Z. B., Ashraf, F., Park, J.-H., and Lim, H.-J.: Volatility parameters of secondary organic aerosol components determined using a thermal denuder, Atmospheric Environment, 226, 117405, 2020.

Barone, G., Della Gatta, G., Ferro, D., and Piacente, V.: Enthalpies and entropies of sublimation, vaporization and fusion of nine polyhydric alcohols, Journal of the Chemical Society, Faraday Transactions, 86, 75-79, 1990.

Bianchi, F., Kurten, T., Riva, M., Mohr, C., Rissanen, M. P., Roldin, P., Berndt, T., Crounse, J. D., Wennberg, P. O., Mentel, T. F., Wildt, J., Junninen, H., Jokinen, T., Kulmala, M., Worsnop, D. R., Thornton, J. A., Donahue, N., Kjaergaard, H. G., and Ehn, M.: Highly oxygenated organic molecules (HOM) from gas-phase autoxidation involving peroxy radicals: A key contributor to atmospheric aerosol, Chem Rev, 119, 3472-3509, 10.1021/acs.chemrev.8b00395, 2019.

Bilde, M., Svenningsson, B., Mønster, J., and Rosenørn, T.: Even− odd alternation of evaporation rates and vapor pressures of C_3− C_9 dicarboxylic acid aerosols, Environmental science & technology, 37, 1371-1378, 2003.

Bilde, M., Barsanti, K., Booth, M., Cappa, C. D., Donahue, N. M., Emanuelsson, E. U., McFiggans, G., Krieger, U. K., Marcolli, C., Topping, D., Ziemann, P., Barley, M., Clegg, S., Dennis-Smither, B., Hallquist, M., Hallquist, A. M., Khlystov, A., Kulmala, M., Mogensen, D., Percival, C. J., Pope, F., Reid, J. P., Ribeiro da Silva, M. A., Rosenoern, T., Salo, K., Soonsin, V. P., Yli-Juuti, T., Prisle, N. L., Pagels, J., Rarey, J., Zardini, A. A., and Riipinen, I.: Saturation vapor pressures and transition enthalpies of low-volatility organic molecules of atmospheric relevance: From dicarboxylic acids to complex mixtures, Chem Rev, 115, 4115-4156, 10.1021/cr5005502, 2015.

BIOVIA COSMO*conf*: Release 2021; dassault systèmes, 2021.

BIOVIA COSMO*therm*: Release 2021; dassault systèmes, 2021.

Booth, A., Markus, T., Mcfiggans, G., Percival, C., Mcgillen, M., and Topping, D.: Design and construction of a simple knudsen effusion mass spectrometer (KEMS) system for vapour pressure measurements of low volatility organics, Atmospheric Measurement Techniques, 2, 355-361, 2009.

490 Bruns, E. A., Greaves, J., and Finlayson-Pitts, B. J.: Measurement of vapor pressures and heats of sublimation of dicarboxylic acids using atmospheric solids analysis probe mass spectrometry, J Phys Chem A, 116, 5900-5909, 10.1021/jp210021f, 2012.

Buchholz, A., Lambe, A. T., Ylisirniö, A., Li, Z., Tikkanen, O.-P., Faiola, C., Kari, E., Hao, L., Luoma, O., Huang, W., Mohr, C., Worsnop, D. R., Nizkorodov, S. A., Yli-Juuti, T., Schobesberger, S., and Virtanen, A.: Insights into
495 the O : C-dependent mechanisms controlling the evaporation of α-pinene secondary organic aerosol particles, Atmospheric Chemistry and Physics, 19, 4061-4073, 10.5194/acp-19-4061-2019, 2019.

Cai, C., Stewart, D. J., Reid, J. P., Zhang, Y. H., Ohm, P., Dutcher, C. S., and Clegg, S. L.: Organic component vapor pressures and hygroscopicities of aqueous aerosol measured by optical tweezers, J Phys Chem A, 119, 704-718, 10.1021/jp510525r, 2015.

500 Cain, K. P., Karnezi, E., and Pandis, S. N.: Challenges in determining atmospheric organic aerosol volatility distributions using thermal evaporation techniques, Aerosol Science and Technology, 54, 941-957, 2020.

Cappa, C. D., Lovejoy, E. R., and Ravishankara, A.: Determination of evaporation rates and vapor pressures of very low volatility compounds: A study of the C_4-C_{10} and C_{12} dicarboxylic acids, The Journal of Physical Chemistry A, 111, 3099-3109, 2007.

505 Cappa, C. D., Lovejoy, E. R., and Ravishankara, A. R.: Evaporation rates and vapor pressures of the even-numbered C8-C18 monocarboxylic acids, J Phys Chem A, 112, 3959-3964, 10.1021/jp710586m, 2008.

Chattopadhyay, S. and Ziemann, P. J.: Vapor pressures of substituted and unsubstituted monocarboxylic and dicarboxylic acids measured using an improved thermal desorption particle beam mass spectrometry method, Aerosol Science and Technology, 39, 1085-1100, 2005.

510 Cheng, Y., Su, H., Koop, T., Mikhailov, E., and Poschl, U.: Size dependence of phase transitions in aerosol nanoparticles, Nat Commun, 6, 5923, 10.1038/ncomms6923, 2015.

Compernolle, S., Ceulemans, K., and Müller, J.-F.: Evaporation: A new vapour pressure estimation methodfor organic molecules including non-additivity and intramolecular interactions, Atmospheric Chemistry and Physics, 11, 9431-9450, 2011.

515 da Silva, M. A. R., Monte, M. J., and Ribeiro, J. R.: Thermodynamic study on the sublimation of succinic acid and of methyl-and dimethyl-substituted succinic and glutaric acids, The Journal of Chemical Thermodynamics, 33, 23-31, 2001.

Dang, C., Bannan, T., Shelley, P., Priestley, M., Worrall, S. D., Waters, J., Coe, H., Percival, C. J., and Topping, D.: The effect of structure and isomerism on the vapor pressures of organic molecules and its potential atmospheric
520 relevance, Aerosol Science and Technology, 53, 1040-1055, 2019.

Davies, M. and Malpass, V.: 212. Heats of sublimation of straight-chain monocarboxylic acids, Journal of the Chemical Society (Resumed), 1048-1055, 1961.

Donahue, N. M., Epstein, S., Pandis, S. N., and Robinson, A. L.: A two-dimensional volatility basis set: 1. Organic-aerosol mixing thermodynamics, Atmospheric Chemistry and Physics, 11, 3303-3318, 2011.

525 Eckert, F. and Klamt, A.: Fast solvent screening via quantum chemistry: COSMO-RS approach, AIChE Journal, 48, 369-385, 2002.

Ehn, M., Thornton, J. A., Kleist, E., Sipila, M., Junninen, H., Pullinen, I., Springer, M., Rubach, F., Tillmann, R., Lee, B., Lopez-Hilfiker, F., Andres, S., Acir, I. H., Rissanen, M., Jokinen, T., Schobesberger, S., Kangasluoma, J.,

Kontkanen, J., Nieminen, T., Kurten, T., Nielsen, L. B., Jorgensen, S., Kjaergaard, H. G., Canagaratna, M., Maso, M. D., Berndt, T., Petaja, T., Wahner, A., Kerminen, V. M., Kulmala, M., Worsnop, D. R., Wildt, J., and Mentel, T. F.: A large source of low-volatility secondary organic aerosol, Nature, 506, 476-479, 10.1038/nature13032, 2014.

Eichler, P., Müller, M., D'anna, B., and Wisthaler, A.: A novel inlet system for online chemical analysis of semi-volatile submicron particulate matter, Atmospheric Measurement Techniques, 8, 1353-1360, 2015.

Emanuelsson, E. U., Tschiskale, M., and Bilde, M.: Phase state and saturation vapor pressure of submicron particles of meso-erythritol at ambient conditions, The Journal of Physical Chemistry A, 120, 7183-7191, 2016.

Fuchs, N. and Sutugin, A.: High-dispersed aerosols, in: Topics in current aerosol research, Elsevier, 1, 1971.

Fuller, E. N., Schettler, P. D., and Giddings, J. C.: New method for prediction of binary gas-phase diffusion coefficients, Industrial & Engineering Chemistry, 58, 18-27, 1966.

Goldfarb, J. L. and Suuberg, E. M.: Vapor pressures and thermodynamics of oxygen-containing polycyclic aromatic hydrocarbons measured using knudsen effusion, Environ Toxicol Chem, 27, 1244-1249, 10.1897/07-486, 2008.

Hallquist, M., Wenger, J. C., Baltensperger, U., Rudich, Y., Simpson, D., Claeys, M., Dommen, J., Donahue, N. M., George, C., Goldstein, A. H., Hamilton, J. F., Herrmann, H., Hoffmann, T., Iinuma, Y., Jang, M., Jenkin, M. E., Jimenez, J. L., Kiendler-Scharr, A., Maenhaut, W., McFiggans, G., Mentel, T. F., Monod, A., Prévôt, A. S. H., Seinfeld, J. H., Surratt, J. D., Szmigielski, R., and Wildt, J.: The formation, properties and impact of secondary organic aerosol: Current and emerging issues, Atmospheric Chemistry and Physics, 9, 5155-5236, 10.5194/acp-9-5155-2009, 2009.

Holzinger, R., Williams, J., Herrmann, F., Lelieveld, J., Donahue, N., and Röckmann, T.: Aerosol analysis using a thermal-desorption proton-transfer-reaction mass spectrometer (TD-PTR-MS): A new approach to study processing of organic aerosols, Atmospheric chemistry and physics, 10, 2257-2267, 2010.

Huang, W., Saathoff, H., Pajunoja, A., Shen, X., Naumann, K.-H., Wagner, R., Virtanen, A., Leisner, T., and Mohr, C.: α-Pinene secondary organic aerosol at low temperature: Chemical composition and implications for particle viscosity, Atmospheric Chemistry and Physics, 18, 2883-2898, 2018.

Hyttinen, N., Pullinen, I., Nissinen, A., Schobesberger, S., Virtanen, A., and Yli-Juuti, T.: Comparison of saturation vapor pressures of α-pinene+O_3 oxidation products derived from COSMO-RS computations and thermal desorption experiments, Atmospheric Chemistry and Physics, 22, 1195-1208, 2022.

Hyttinen, N., Wolf, M., Rissanen, M. P., Ehn, M., Perakyla, O., Kurtén, T., and Prisle, N. L.: Gas-to-particle partitioning of cyclohexene-and α-pinene-derived highly oxygenated dimers evaluated using COSMOtherm, The Journal of Physical Chemistry A, 125, 3726-3738, 2021.

Jimenez, J. L., Canagaratna, M. R., Donahue, N. M., Prevot, A. S., Zhang, Q., Kroll, J. H., DeCarlo, P. F., Allan, J. D., Coe, H., Ng, N. L., Aiken, A. C., Docherty, K. S., Ulbrich, I. M., Grieshop, A. P., Robinson, A. L., Duplissy, J., Smith, J. D., Wilson, K. R., Lanz, V. A., Hueglin, C., Sun, Y. L., Tian, J., Laaksonen, A., Raatikainen, T., Rautiainen, J., Vaattovaara, P., Ehn, M., Kulmala, M., Tomlinson, J. M., Collins, D. R., Cubison, M. J., Dunlea, E. J., Huffman, J. A., Onasch, T. B., Alfarra, M. R., Williams, P. I., Bower, K., Kondo, Y., Schneider, J., Drewnick, F., Borrmann, S., Weimer, S., Demerjian, K., Salcedo, D., Cottrell, L., Griffin, R., Takami, A., Miyoshi, T., Hatakeyama, S., Shimono, A., Sun, J. Y., Zhang, Y. M., Dzepina, K., Kimmel, J. R., Sueper, D., Jayne, J. T., Herndon, S. C., Trimborn, A. M., Williams, L. R., Wood, E. C., Middlebrook, A. M., Kolb, C. E., Baltensperger,

U., and Worsnop, D. R.: Evolution of organic aerosols in the atmosphere, Science, 326, 1525-1529, 10.1126/science.1180353, 2009.

570 Julin, J., Winkler, P. M., Donahue, N. M., Wagner, P. E., and Riipinen, I.: Near-unity mass accommodation coefficient of organic molecules of varying structure, Environ Sci Technol, 48, 12083-12089, 10.1021/es501816h, 2014.

Kerminen, V.-M., Paramonov, M., Anttila, T., Riipinen, I., Fountoukis, C., Korhonen, H., Asmi, E., Laakso, L., Lihavainen, H., and Swietlicki, E.: Cloud condensation nuclei production associated with atmospheric nucleation:

575 A synthesis based on existing literature and new results, Atmospheric Chemistry and Physics, 12, 12037-12059, 2012.

Klamt, A.: Conductor-like screening model for real solvents: A new approach to the quantitative calculation of solvation phenomena, The Journal of Physical Chemistry, 99, 2224-2235, 1995.

Klamt, A., Jonas, V., Bürger, T., and Lohrenz, J. C.: Refinement and parametrization of COSMO-RS, The Journal

580 of Physical Chemistry A, 102, 5074-5085, 1998.

Klinger, E., Rickert, D., and Hasenauer, J.: pyABC: Distributed, likelihood-free inference, Bioinformatics, 34, 3591-3593, 10.1093/bioinformatics/bty361, 2018.

Koponen, I. K., Riipinen, I., Hienola, A., Kulmala, M., and Bilde, M.: Thermodynamic properties of malonic, succinic, and glutaric acids: Evaporation rates and saturation vapor pressures, Environ Sci Technol, 41, 3926-3933,

585 10.1021/es0611240, 2007.

Krechmer, J. E., Day, D. A., Ziemann, P. J., and Jimenez, J. L.: Direct measurements of gas/particle partitioning and mass accommodation coefficients in environmental chambers, Environ Sci Technol, 51, 11867-11875, 10.1021/acs.est.7b02144, 2017.

Krieger, U. K., Siegrist, F., Marcolli, C., Emanuelsson, E. U., Gøbel, F. M., Bilde, M., Marsh, A., Reid, J. P.,

590 Huisman, A. J., Riipinen, I., Hyttinen, N., Myllys, N., Kurtén, T., Bannan, T., Percival, C. J., and Topping, D.: A reference data set for validating vapor pressure measurement techniques: Homologous series of polyethylene glycols, Atmospheric Measurement Techniques, 11, 49-63, 10.5194/amt-11-49-2018, 2018.

Kurten, T., Tiusanen, K., Roldin, P., Rissanen, M., Luy, J.-N., Boy, M., Ehn, M., and Donahue, N.: α-Pinene autoxidation products may not have extremely low saturation vapor pressures despite high O: C ratios, The Journal

595 of Physical Chemistry A, 120, 2569-2582, 2016.

Kurtén, T., Hyttinen, N., D'Ambro, E. L., Thornton, J., and Prisle, N. L.: Estimating the saturation vapor pressures of isoprene oxidation products $C_5H_{12}O_6$ and $C_5H_{10}O_6$ using COSMO-RS, Atmospheric Chemistry and Physics, 18, 17589-17600, 2018.

Li, W. and Chen, D.-R.: Performance of nano-dma operated with different gases for sheath and aerosol carrier

600 flows, Aerosol Science and Technology, 39, 931-940, 10.1080/02786820500346520, 2005.

Li, Z., Tikkanen, O.-P., Buchholz, A., Hao, L., Kari, E., Yli-Juuti, T., and Virtanen, A.: Effect of decreased temperature on the evaporation of α-pinene secondary organic aerosol particles, ACS Earth and Space Chemistry, 3, 2775-2785, 2019.

Li, Z., Buchholz, A., Barreira, L. M. F., Ylisirniö, A., Hao, L., Pullinen, I., Schobesberger, S., and Virtanen, A.:

605 Isothermal evaporation of α-pinene secondary organic aerosol particles formed under low NO_x and high NO_x conditions, Atmospheric Chemistry and Physics, 23, 203-220, 10.5194/acp-23-203-2023, 2023.

Li, Z., Buchholz, A., Ylisirniö, A., Barreira, L., Hao, L., Schobesberger, S., Yli-Juuti, T., and Virtanen, A.: Evolution of volatility and composition in sesquiterpene-mixed and α-pinene secondary organic aerosol particles during isothermal evaporation, Atmospheric Chemistry and Physics, 21, 18283-18302, 10.5194/acp-21-18283-2021, 2021.

Liepe, J., Kirk, P., Filippi, S., Toni, T., Barnes, C. P., and Stumpf, M. P.: A framework for parameter estimation and model selection from experimental data in systems biology using approximate bayesian computation, Nat Protoc, 9, 439-456, 10.1038/nprot.2014.025, 2014.

Liu, X., Day, D. A., Krechmer, J. E., Ziemann, P. J., and Jimenez, J. L.: Determining activity coefficients of SOA from isothermal evaporation in a laboratory chamber, Environmental Science & Technology Letters, 8, 212-217, 2020.

Liu, X., Day, D. A., Krechmer, J. E., Brown, W., Peng, Z., Ziemann, P. J., and Jimenez, J. L.: Direct measurements of semi-volatile organic compound dynamics show near-unity mass accommodation coefficients for diverse aerosols, Communications Chemistry, 2, 98, 2019.

Lopez-Hilfiker, F. D., Mohr, C., Ehn, M., Rubach, F., Kleist, E., Wildt, J., Mentel, T. F., Lutz, A., Hallquist, M., Worsnop, D., and Thornton, J. A.: A novel method for online analysis of gas and particle composition: Description and evaluation of a filter inlet for gases and aerosols (FIGAERO), Atmospheric Measurement Techniques, 7, 983-1001, 10.5194/amt-7-983-2014, 2014.

Mitchem, L. and Reid, J. P.: Optical manipulation and characterisation of aerosol particles using a single-beam gradient force optical trap, Chem Soc Rev, 37, 756-769, 10.1039/b609713h, 2008.

Mohr, C., Thornton, J. A., Heitto, A., Lopez-Hilfiker, F. D., Lutz, A., Riipinen, I., Hong, J., Donahue, N. M., Hallquist, M., Petaja, T., Kulmala, M., and Yli-Juuti, T.: Molecular identification of organic vapors driving atmospheric nanoparticle growth, Nat Commun, 10, 4442, 10.1038/s41467-019-12473-2, 2019.

Moore, W.: Electrochemistry: Conductance and ionic reactions, Physical chemistry, 1962.

Nannoolal, Y., Rarey, J., and Ramjugernath, D.: Estimation of pure component properties: Part 3. Estimation of the vapor pressure of non-electrolyte organic compounds via group contributions and group interactions, Fluid Phase Equilibria, 269, 117-133, 2008.

Pankow, J. F.: An absorption model of gas/particle partitioning of organic compounds in the atmosphere, Atmospheric Environment, 28, 185-188, 10.1016/1352-2310(94)90093-0, 1994.

Pankow, J. F. and Asher, W. E.: SIMPOL. 1: A simple group contribution method for predicting vapor pressures and enthalpies of vaporization of multifunctional organic compounds, Atmospheric Chemistry and Physics, 8, 2773-2796, 2008.

Price, C. L., Kaur Kohli, R., Shokoor, B., and Davies, J. F.: Connecting the phase state and volatility of dicarboxylic acids at elevated temperatures, The Journal of Physical Chemistry A, 126, 6963-6972, 2022.

Rader, D., McMurry, P. H., and Smith, S.: Evaporation rates of monodisperse organic aerosols in the 0.02-to 0.2-μm-diameter range, Aerosol science and technology, 6, 247-260, 1987.

Reid, R. C., Prausnitz, J. M., and Poling, B. E.: The properties of gases and liquids, 4th ed., McGraw Hill Book Co, New York, 1987.

645 Riipinen, I., Svenningsson, B., Bilde, M., Gaman, A., Lehtinen, K., and Kulmala, M.: A method for determining thermophysical properties of organic material in aqueous solutions: Succinic acid, Atmospheric research, 82, 579-590, 2006.

Saha, P. K., Khlystov, A., and Grieshop, A. P.: Determining aerosol volatility parameters using a "dual thermodenuder" system: Application to laboratory-generated organic aerosols, Aerosol Science and Technology, 49, 620-632, 2015.

650 Saleh, R., Khlystov, A., and Shihadeh, A.: Effect of aerosol generation method on measured saturation pressure and enthalpy of vaporization for dicarboxylic acid aerosols, Aerosol Science and Technology, 44, 302-307, 10.1080/02786821003591810, 2010.

Saleh, R., Walker, J., and Khlystov, A.: Determination of saturation pressure and enthalpy of vaporization of semi-volatile aerosols: The integrated volume method, J Aerosol Sci, 39, 876-887, 10.1016/j.jaerosci.2008.06.004, 2008.

655 Salo, K., Jonsson, A. M., Andersson, P. U., and Hallquist, M.: Aerosol volatility and enthalpy of sublimation of carboxylic acids, J Phys Chem A, 114, 4586-4594, 10.1021/jp910105h, 2010.

Schälte, Y. and Hasenauer, J.: Efficient exact inference for dynamical systems with noisy measurements using sequential approximate bayesian computation, Bioinformatics, 36, i551-i559, 2020.

Schobesberger, S., D'Ambro, E. L., Lopez-Hilfiker, F. D., Mohr, C., and Thornton, J. A.: A model framework to 660 retrieve thermodynamic and kinetic properties of organic aerosol from composition-resolved thermal desorption measurements, Atmospheric Chemistry and Physics, 18, 14757-14785, 10.5194/acp-18-14757-2018, 2018.

Schwantes, R. H., Charan, S. M., Bates, K. H., Huang, Y., Nguyen, T. B., Mai, H., Kong, W., Flagan, R. C., and Seinfeld, J. H.: Low-volatility compounds contribute significantly to isoprene secondary organic aerosol (SOA) under high-NO_x conditions, Atmospheric Chemistry and Physics, 19, 7255-7278, 2019.

665 Shelley, P. D., Bannan, T. J., Worrall, S. D., Alfarra, M. R., Krieger, U. K., Percival, C. J., Garforth, A., and Topping, D.: Measured solid state and subcooled liquid vapour pressures of nitroaromatics using knudsen effusion mass spectrometry, Atmospheric Chemistry and Physics, 20, 8293-8314, 2020.

Sisson, S. A., Fan, Y., and Tanaka, M. M.: Sequential monte carlo without likelihoods, Proceedings of the National Academy of Sciences, 104, 1760-1765, 2007.

670 Stahn, M., Grimme, S., Salthammer, T., Hohm, U., and Palm, W. U.: Quantum chemical calculation of the vapor pressure of volatile and semi volatile organic compounds, Environ Sci Process Impacts, 24, 2153-2166, 10.1039/d2em00271j, 2022.

Tao, Y. and McMurry, P. H.: Vapor pressures and surface free energies of C_{14}-C_{18} monocarboxylic acids and C_5 and C_6 dicarboxylic acids, Environmental science & technology, 23, 1519-1523, 1989.

675 Toni, T., Welch, D., Strelkowa, N., Ipsen, A., and Stumpf, M. P.: Approximate bayesian computation scheme for parameter inference and model selection in dynamical systems, J R Soc Interface, 6, 187-202, 10.1098/rsif.2008.0172, 2009.

TURBOMOLE, V.: V7.4.1, a development of University of Karlsruhe and Forschungszentrum Karlsruhe GmbH, 1989–2007, TURBOMOLE GmbH, since 2007, 2019.

680 von Domaros, M., Lakey, P. S. J., Shiraiwa, M., and Tobias, D. J.: Multiscale modeling of human skin oil-induced indoor air chemistry: Combining kinetic models and molecular dynamics, J Phys Chem B, 124, 3836-3843, 10.1021/acs.jpcb.0c02818, 2020.

Yang, L. H., Takeuchi, M., Chen, Y., and Ng, N. L.: Characterization of thermal decomposition of oxygenated organic compounds in FIGAERO-CIMS, Aerosol Science and Technology, 55, 1321-1342, 10.1080/02786826.2021.1945529, 2021.

Yatavelli, R. L. and Thornton, J. A.: Particulate organic matter detection using a micro-orifice volatilization impactor coupled to a chemical ionization mass spectrometer (MOVI-CIMS), Aerosol Science and Technology, 44, 61-74, 2010.

Yeung, M. C., Ling, T. Y., and Chan, C. K.: Effects of the polymorphic transformation of glutaric acid particles on their deliquescence and hygroscopic properties, The Journal of Physical Chemistry A, 114, 898-903, 2010.

Yli-Juuti, T., Zardini, A. A., Eriksson, A. C., Hansen, A. M., Pagels, J. H., Swietlicki, E., Svenningsson, B., Glasius, M., Worsnop, D. R., Riipinen, I., and Bilde, M.: Volatility of organic aerosol: Evaporation of ammonium sulfate/succinic acid aqueous solution droplets, Environ Sci Technol, 47, 12123-12130, 10.1021/es401233c, 2013.

Yli-Juuti, T., Pajunoja, A., Tikkanen, O. P., Buchholz, A., Faiola, C., Vaisanen, O., Hao, L., Kari, E., Perakyla, O., Garmash, O., Shiraiwa, M., Ehn, M., Lehtinen, K., and Virtanen, A.: Factors controlling the evaporation of secondary organic aerosol from alpha-pinene ozonolysis, Geophys Res Lett, 44, 2562-2570, 10.1002/2016GL072364, 2017.

Ylisirniö, A., Barreira, L. M. F., Pullinen, I., Buchholz, A., Jayne, J., Krechmer, J. E., Worsnop, D. R., Virtanen, A., and Schobesberger, S.: On the calibration of FIGAERO-ToF-CIMS: Importance and impact of calibrant delivery for the particle-phase calibration, Atmospheric Measurement Techniques, 14, 355-367, 10.5194/amt-14-355-2021, 2021.

Zardini, A. A. and Krieger, U. K.: Evaporation kinetics of a non-spherical, levitated aerosol particle using optical resonance spectroscopy for precision sizing, Opt Express, 17, 4659-4669, 10.1364/oe.17.004659, 2009.

Zardini, A. A., Krieger, U. K., and Marcolli, C.: White light mie resonance spectroscopy used to measure very low vapor pressures of substances in aqueous solution aerosol particles, Optics Express, 14, 6951-6962, 2006.

Zhang, Q., Jimenez, J., Canagaratna, M., Allan, J., Coe, H., Ulbrich, I., Alfarra, M., Takami, A., Middlebrook, A., and Sun, Y.: Ubiquity and dominance of oxygenated species in organic aerosols in anthropogenically‑influenced northern hemisphere midlatitudes, Geophysical Research Letters, 34, 2007.